Generalized stability criteria for power amplifiers under mismatch effects

Almudena Suárez, *Fellow, IEEE,* Franco Ramírez, *Member, IEEE,* Sergio Sancho, *Member, IEEE*

***Abstract*— Potential instability of power amplifiers (PAs) under mismatch effects is analysed, with emphasis on the ease and generality of application of the stability criteria. The methodology is based on the evaluation of a large-signal version of the μ factor, considering mismatch effects in the fundamental frequency and three relevant sidebands: the baseband, the lower sideband and the upper sideband. This requires an outer-tier scattering-type conversion matrix of order 3×3 to be obtained, with the rest of sideband equations acting as an inner tier. It is taken into account that the circuit behaves nonlinearly with respect to the termination at the fundamental frequency. The consideration of three sidebands will enable the prediction of the two major forms of large-signal instability: incommensurable oscillations and frequency divisions by two. The analysis is preceded by an evaluation of the circuit own stability properties (*proviso*) under open and short circuit terminations at the sidebands, for all possible values of the termination at the fundamental frequency. Three different μ factors can be defined between any two ports of the scattering matrix. The analysis of the relationships between these factors and their continuity properties will allow the derivation of a single number able to characterize the PA potential instability for each fundamental-frequency termination. Results have been exhaustively validated with independent circuit-level simulations based on pole-zero identification and with measurements, using a variable output load and loading the PA with an antenna.**

***Index Terms*— Stability analysis, bifurcation, antenna mismatch.**

I. Introduction

Instability of power amplifiers (PAs) under termination conditions other than 50 Ω, usually due to antenna mismatch [1]–[4], can give rise to severe malfunctioning, as reported in many previous works [5]–[11]. Furthermore, some applications impose stable operation even under highly reflective loads [6], [8]. The stability analysis under output mismatch is involved since it must be carried out under unknown termination impedances. To be precise, the practical stability analysis of a periodic solution with harmonic components kf_{in}, where k goes from $-N$ to N, is based on the introduction of a perturbation at the positive frequency f [12]–[15], which will give rise, through mixing effects, to the sideband frequencies $kf_{in}+f$. The aim is to predict the reaction of the periodic solution to small perturbations, so the circuit will be linearized about this solution and its frequency response will be obtained by sweeping f. Under mismatched conditions, the frequency-dependent load impedance will exhibit unknown values at kf_{in} and $kf_{in}+f$, where $|k| \le N$. However, some considerations can be made. In the PA, the harmonic amplitudes are generally significant at the device output terminals, but quite low at the final 50 Ω termination of the output network [16]–[23]. For instance, in a Class-E amplifier [16]–[17] a nearly sinusoidal fundamental-frequency current flows through the output series resonator, so the impedance at the fundamental frequency is the most influential one. As stated in [17], the load network may include a low-pass or a band-pass filter to suppress harmonics of the switching frequency at the final output 50 Ω load [19]–[20]. On the other hand, in a class–F amplifier [21]–[23] the output network forces the output voltage to be ideally sinusoidal and additional resonators are added to tune the harmonic components. The mismatch effects occur after the PA output network, at the reference plane indicated in Fig. 1(a), so, in general, they will have a negligible effect at harmonic frequencies kf_{in}, where $|k| \ge 2$.

Taking all the above into account, the approach in [9]–[11] assumes a bandpass filtering action of the PA output network, such that the particular values of the load impedances at frequencies other than the fundamental frequency f_{in} and its lower and upper sidebands, $f_l = f_{in} - f$ and $f_u = f_{in} + f$, have a negligible impact on the stability properties. With this in mind, the analysis of mismatch effects is limited to the three frequencies f_{in}, f_l, f_u, at which the termination impedances may take any value. Then, a two-tier conversion matrix analysis is carried out [10]–[11]. The outer-tier system is based on a 2×2 scattering-type matrix at the two mismatched sideband frequencies $f_l^* = -f_{in} + f$ and f_u, defined at the PA termination plane. The inner-tier system accounts for the rest of sideband frequencies, whose termination impedance values should have a negligible impact on the stability properties. Thus, they can be arbitrarily terminated in 50 Ω.

The two sideband frequencies f_l^* and f_u act as two virtual ports, which has enabled the extension of the Rollet stability criteria [24]–[25] to large-signal operation under output mismatch effects [10]. However, [10] assumed a particular (matched) termination condition $\Gamma_o = 0$ at the fundamental

Manuscript received July 1, 2015. This work has been supported by the Spanish Government under contract TEC2014-60283-C3-1-R and the Parliament of Cantabria (12.JP02.64069). This paper is an expanded version from the IEEE MTT-S International Microwave Symposium, Phoenix, AZ, USA, 17-22 May 2015.

The authors are with the Communications Engineering Department, University of Cantabria, Santander, Spain. (suareza@unican.es; ramirezf@unican.es; sanchosm@unican.es).

frequency f_{in}. The generalization to arbitrary Γ_o terminations implies some analysis difficulties, since any change of Γ_o leads to a different steady-state solution, which must be calculated with harmonic balance (HB). Practical use and interpretation of data resulting from multiple amplitude and phase sweeps in Γ_o require a judicious technique. In this sense, [11] proposed the calculation of a large-signal μ_{LS} factor, obtained from the outer-tier scattering-type matrix at f_l^* and f_u, and the use of constant-μ_{LS} contours, traced on the Smith chart corresponding to Γ_o (with respect to which the circuit behaves nonlinearly). A limitation of this method lies in the fact that only particular values of the perturbation frequency *f* are considered, though the stability analysis of a periodic regime at f_{in}, must take into account all the *f* values between 0 and $f_{in}/2$. In fact, an upper frequency higher than $f_{in}/2$ will be necessary to detect the subharmonic resonance leading to a frequency division by 2, which is one of the main forms of large-signal instability [26]. In view of this problem, one of the objectives here will be derivation of a new analysis method accounting for this whole interval of perturbation frequencies.

In [11], a preliminary investigation including the baseband termination in the set of relevant mismatched terminations was presented. This relied on the calculation of a 3×3 outer-tier scattering matrix at the three sideband frequencies $f_b = f$, f_l^* and f_u. However, the three-sideband analysis in [11] was only used for a final validation of the results obtained with the 2×2 scattering matrix, due to the difficulties involved in the evaluation of the large-signal μ_{LS} for three possible combinations of two sidebands, (f_b, f_l^*), (f_b, f_u) and (f_l^*, f_u), considering, in each case, all possible values of the complex reflection coefficient at the remaining sideband, denoted as Γ_{sb}. Furthermore, the evaluation of each large-signal μ_{LS} must be carried out for each fundamental-frequency termination Γ_o and each perturbation frequency *f*, which will lead to prohibitive computational cost, unless some useful mathematical properties are identified.

This work will present a thorough methodology for the stability analysis of PAs under mismatch effects that is mathematically consistent for all the possible values of the perturbation frequency *f*. It will be derived from an in-depth investigation of the relationships between the different μ_{LS} factors that can be defined in a three-sideband analysis, and a detailed study of their frequency dependences. The aim will be to obtain a single real quantity $\mu_{LS}^T(\Gamma_o)$ defining the PA potential stability properties in the whole perturbation-frequency interval, for each termination Γ_o at f_{in}. Unlike the two-sideband case, the analysis at f_b, f_l^*, f_u accurately deals with situations in which the dangerous frequency intervals in f_b and f_l are close to $f_{in}/2$ or comprise this frequency. Therefore, it should enable a prediction of frequency divisions by two, often encountered in unstable PAs [27]–[28].

This work will also take into account the need to verify the fulfilment of a *proviso*, with identical meaning to Rollet's proviso [29]–[30] in a small-signal analysis, ensuring the observability of mismatched-induced instabilities from the output reference plane. This will require verification of the circuit stability under both open and short circuit terminations at the three relevant sidebands for all the possible values of the fundamental-frequency termination Γ_o. The analysis strategy, based on pole-zero identification, will take advantage of the continuity of the circuit equations, in order to avoid an unmanageable amount of data of difficult interpretation. The methods will be illustrated by means of its application to a PA at $f_{in} = 0.8$ GHz with 80% efficiency at 22 dBm output power.

The paper is organized as follows. Section II presents the calculation of the three-sideband scattering matrix. Section III describes the potential instability analysis at three sidebands. Section IV presents a validation based on the calculation of stability circles. Section V proposes a new global stability parameter that is exhaustively validated with measurements.

II. Calculation of the Three-Sideband Scattering Matrix

The stability analysis of a periodic solution at f_{in} relies on the introduction of a perturbation at a frequency *f*, to obtain the frequency response of the circuit linearized about this solution [12]. This will give rise to the mixing frequencies $kf_{in} + f$, where *k* goes from *–N* to *N* [12]–[15], [31]–[32]. The opposite frequencies $-kf_{in} - f$, though not considered in the analysis, will also exist and their components will be complex-conjugates of those at $kf_{in} + f$. In the case of a stability analysis under output mismatch effects, and taking into account the low-pass characteristic of the output network, the mismatched conditions at the output reference plane [Fig. 1(a)] can be restricted to the fundamental frequency f_{in} and the three frequencies $f_b = f$, $f_l^* = -f_{in} + f$ and $f_u = f_{in} + f$. These mismatched frequencies are respectively terminated in the arbitrary reflection coefficients $\Gamma_o, \Gamma_b, \Gamma_l^*, \Gamma_u$ at each perturbation frequency *f* [Fig. 1(a)]. The load impedances at the rest of the harmonic frequencies kf_{in} and sideband frequencies $kf_{in} + f$, where $k \neq 0, -1, 1$, should have no impact on the stability properties and can be arbitrarily terminated in $Z_c = 50\,\Omega$. Note that the analysis method takes into account all the harmonic and sideband frequencies without any restrictions. The sole assumption is that mismatch effects (at the reference plane, after the output network) are only relevant at f_{in}, $f_b = f$, $f_l^* = -f_{in} + f$ and $f_u = f_{in} + f$. Fig. 1(b) shows a sketch of the analysis frequencies and the termination impedances at the output reference plane, with the harmonic components in a solid line and the sideband frequencies in a dashed line.

For each termination Γ_o at the fundamental frequency f_{in}, a full HB analysis is carried out considering *N* harmonic terms. Next, the circuit is linearized about the resulting steady-state solution with the conversion-matrix approach [31]–[33]. The circuit's linearized equations are decomposed into an outer-tier system at f_b, f_l^*, f_u and an inner-tier system at the rest of the frequencies $kf_{in} + f$, where $k \neq 0, -1, 1$, terminated in

$Z_c = 50\,\Omega$. The outer-tier system is formulated at the circuit's output reference plane [Fig. 1(a)] by means of 3×3 impedance matrix [Z_3], later transformed into a scattering matrix. The [Z_3] matrix is obtained through the simultaneous conversion-matrix analysis of three circuits, terminated in Γ_o at f_{in}, in open circuit at f, $-f_{in}+f$ and $f_{in}+f$, and in $\Gamma = 0$ at the rest of the frequency components, as shown in Fig. 2(b). Each circuit will contain an independent small-signal current source at one of the sidebands $I(f)$, $I(-f_{in}+f)$, $I(f_{in}+f)$. Then, the parameters of a 3×3 impedance matrix are obtained from the three respective circuits, as:

$$Z_{bb}=\frac{V(f)}{I(f)},\ Z_{lb}=\frac{V(-f_{in}+f)}{I(f)},\ Z_{ub}=\frac{V(f_{in}+f)}{I(f)}$$
$$Z_{bl}=\frac{V(f)}{I(-f_{in}+f)},\ Z_{ll}=\frac{V(-f_{in}+f)}{I(-f_{in}+f)},\ Z_{ul}=\frac{V(f_{in}+f)}{I(-f_{in}+f)} \qquad (1)$$
$$Z_{bu}=\frac{V(f)}{I(f_{in}+f)},\ Z_{lu}=\frac{V(-f_{in}+f)}{I(f_{in}+f)},\ Z_{uu}=\frac{V(f_{in}+f)}{I(f_{in}+f)}$$

The above calculation is performed with a full conversion matrix approach, taking into account all the sideband frequencies $kf_{in}+f$, where k goes from $-N$ to N. Note that we will have a different impedance matrix [Z_3] for each termination Γ_o at f_{in} and each perturbation frequency f. The system is linear with respect to the terminations at the sideband frequencies, but nonlinear with respect to the termination Γ_o at f_{in}. Thus, a harmonic-balance analysis must be performed for any variation of the termination Γ_o at f_{in}. The (3×3) impedance matrix in (1) can be transformed into a (3×3) matrix of scattering type [S_3], which will relate reflected and incident power waveforms at the three sidebands:

$$\begin{bmatrix} b_b \\ b_l^* \\ b_u \end{bmatrix} = \begin{bmatrix} s_{bb}(\Gamma_o,f) & s_{bl}(\Gamma_o,f) & s_{bu}(\Gamma_o,f) \\ s_{lb}(\Gamma_o,f) & s_{ll}(\Gamma_o,f) & s_{lu}(\Gamma_o,f) \\ s_{ub}(\Gamma_o,f) & s_{ul}(\Gamma_o,f) & s_{uu}(\Gamma_o,f) \end{bmatrix} \begin{bmatrix} a_b \\ a_l^* \\ a_u \end{bmatrix} \qquad (2)$$

where the asterisk denotes complex conjugation. This scattering matrix will allow a generalization of Rollet's criteria [24]–[25] to predict potential instability under mismatch effects. The PA will be potentially unstable under these effects if for any pair of terminations at the sidebands f_l^*, f_u, at the sidebands f_b, f_l^* or at the sidebands f_b, f_u, it exhibits negative resistance when looking into the circuit output at f_b, f_u or f_l^*, respectively. This verification must be performed for every passive termination Γ_o at f_{in} and every perturbation frequency f. However, the analysis described will only be able to detect the circuit instability under fulfilment of the *Rollet proviso* [29]–[30], [34]–[35], which must be adapted here to the problem of three mismatched sideband frequencies.

To fulfil the proviso, the circuit terminated in Γ_o at f_{in} must be stable on its own, or equivalently, it must not exhibit any poles on the right-hand side of the complex plane (RHP) when the three sidebands are in open and short circuit conditions. The proviso must be verified for each passive termination Γ_o at f_{in}, with the three sideband frequencies f, $-f_{in}+f$ and $f_{in}+f$ in all possible combinations of short-circuit and open-circuit terminations. Indeed, short-circuit terminations facilitate the detection of unstable series resonances, which might not be observable from the analysis reference plane, whereas open-circuit terminations facilitate the detection of unstable parallel resonances.

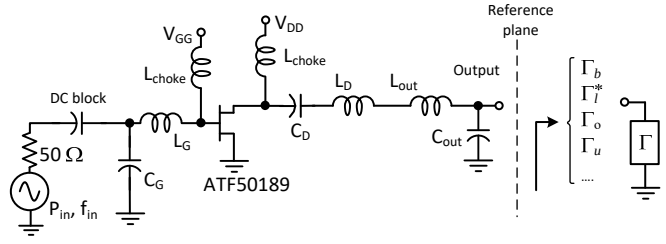

(a)

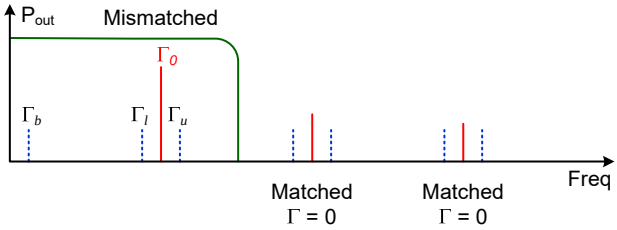

(b)

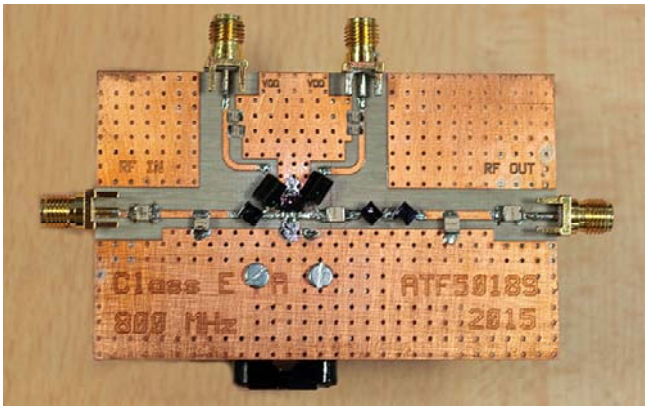

(c)

Fig. 1 Power amplifier under output mismatch effects. The transistor is an Avago ATF-50189, and the element values are L_{choke} = 150 nH, C_D = 2.2 pF, L_D = 18 nH, L_{out} = 12.5 nH, C_{out} = 1.5 pF, L_G = 2.5 nH and C_G = 1.5 pF. In the modified PA, the output inductor is L_{out} = 8 nH. (a) Circuit schematic. (b) Sketch of the termination impedances (replacing the original 50 Ω load) at the analysis frequencies, including harmonics, in a solid line, and sidebands, in a dashed line. (c) Photograph.

The verification of the proviso can be carried out with pole-zero identification [8], [15], fully applicable under open/short circuit terminations, since the load remains fixed at real impedance values at all the sideband frequencies $kf_{in}+f$, given by zero, near infinite or 50 Ω. In fact, any complex-impedance (with a non-zero imaginary part) must physically vary with f, so pole-zero identification should not be applied under constant complex termination impedances at the sideband frequencies. The pole-zero identification will be carried out versus variations in the termination Γ_o at f_{in}.

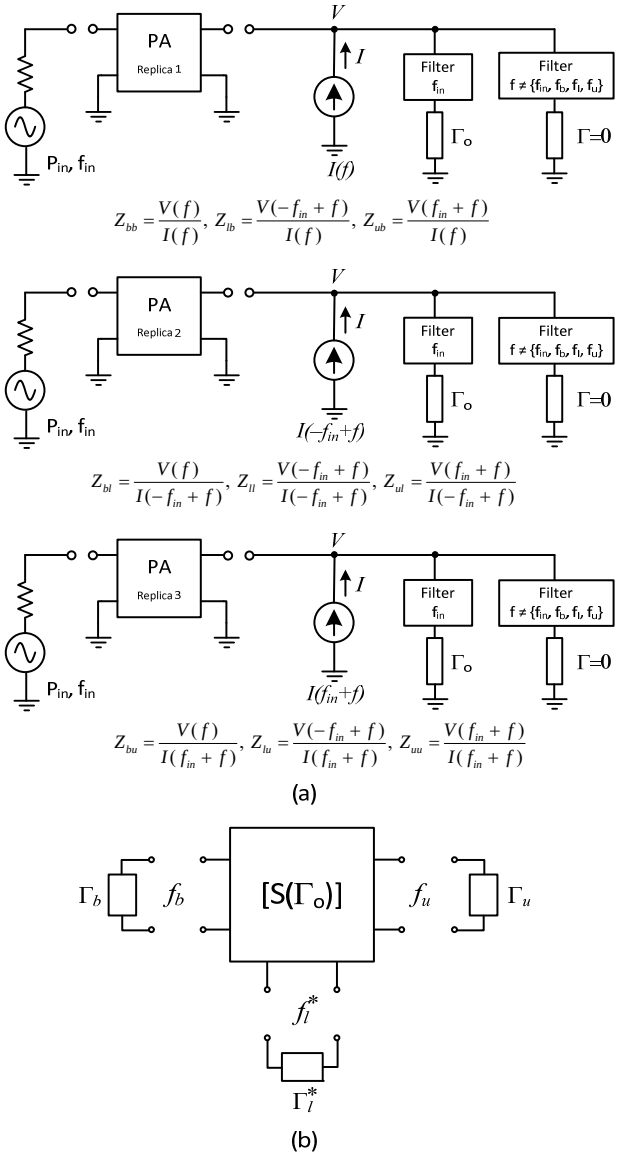

Fig. 2 Two-tier conversion-matrix analysis. For each termination Γ_o at f_{in}, the perturbed circuit is represented with a 3×3 scattering matrix, calculated at the PA output terminals, as shown in Fig. 1. (a) Three circuit replicas used for the calculation of the 3×3 impedance matrix [Z_3]. (b) Sketch of the outer-tier scattering matrix and load impedances at the three sideband frequencies with mismatch effects.

A double sweep in the amplitude and phase of Γ_o provides disconnected circles, which impedes taking advantage of the continuity properties of the harmonic-balance system. Indeed, this set of nonlinear algebraic equations is continuous with respect to all of its variables and parameters [12], [14]. Thus, it will also exhibit a continuous dependence on the load reflection coefficient at the fundamental frequency Γ_o. The analysis can be carried out following a single spiral curve, depending on a single parameter h, which will define both the amplitude and phase of the reflection coefficient $\Gamma_o(h)=0.999h\,e^{j(2N_h\pi+\pi)h}$, $0\le h\le 1$, $N_h=11$. For a smaller h step, and higher values of N_h, the Smith chart will be covered in a finer way. Additionally the unit circle $|\Gamma_o|=1$ can be considered for a detailed analysis of the effect of purely reactive impedances.

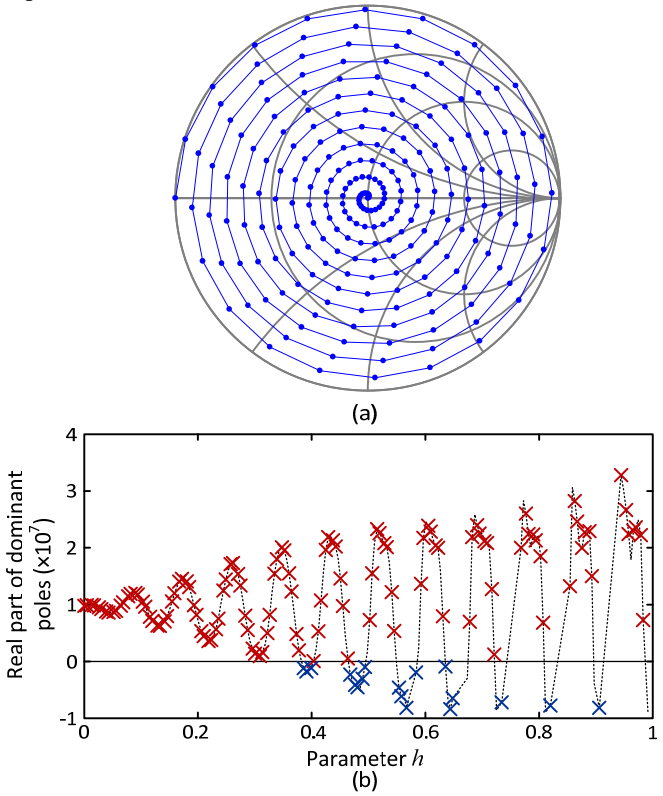

Fig. 3 Application of the proviso to the original PA in Fig. 1, following the spiral curve $\Gamma_o(h)=0.999h\,e^{j(2N\pi+\pi)h}$, $0\le h\le 1$, $N_h=11$ (a) Spiral curve considered, traced on the Smith chart. (b) Pole evolution versus the parameter h in $\Gamma_o(h)$ under short-circuit terminations at the relevant sidebands.

The analysis of the Rollet proviso will be applied to the Class-E PA in Fig. 1(a), with specified output power 22.5 dBm and efficiency 80% at $f_{in}=0.8$ GHz and $P_{in}=12$ dBm. The original values of the output inductor and load resistance are $L_{out}=5$ nH and $R=41.5\,\Omega$. The resistance is implemented through an L-C matching section, terminated in 50 Ω (Fig. 1). The analysis has been carried out with $N=7$ harmonic terms. This number of harmonic terms will be considered through the whole manuscript, for both the circuit-level simulations and the two-tier conversion-matrix analysis, based on [S_3] in (2). Fig. 3(a) shows the spiral considered in the Smith Chart. Fig 3(b) evidences that the circuit does not fulfil the proviso. This figure shows the variation of the real part of the dominant poles versus the parameter h when using short-circuit terminations at the sidebands. When these sidebands are short-circuited, the circuit is unstable even under a 50 Ω termination at f_{in}. Note, however, that it is stable when fully matched, that is, when operating under a 50 Ω final-termination load at all the harmonic and sideband frequencies. With the spiral curve, advantage is taken of the continuity of the circuit equations for an undemanding analysis. To improve the robustness of the circuit under mismatch-induced instability, some modifications have been performed in the output network. The output inductor has been changed to $L_{out}=8$ nH and the new load resistance, also implemented with an L-C section, is $R=45\,\Omega$. When repeating the analysis of the proviso through the spiral curve $\Gamma_o(h)$, the

circuit is stable under open and short circuit terminations at the three relevant sidebands, as shown in Fig, 4. Therefore, the potential instability analysis described in the next section will be applicable.

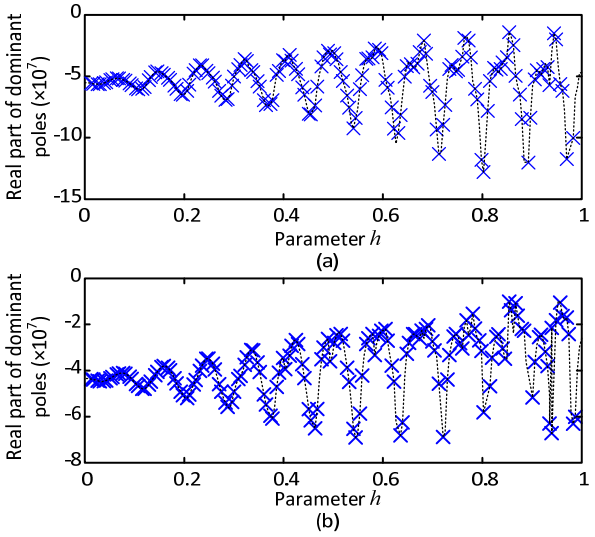

Fig. 4 Application of the proviso to the modified PA with $L_{out} = 8$ nH and $R = 45\ \Omega$, following the spiral curve in Fig. 3a. (a) Under open circuit terminations at the relevant sidebands. (b) Under short-circuit terminations.

III. Potential Instability Analysis at the Three-Sidebands

The works [36]–[37] demonstrate an extension of Rollet's analysis to three-port linear networks, which is based on the sequential definition of three different two-port networks. In each case, the two ports are taken from those of the original three-port network, under a variable passive termination Γ in the remaining port. In [11], this procedure is adapted to the three-band stability analysis under mismatch effects. Under a termination Γ_{sb} at any of the three sideband frequencies $f, -f_{in}+f, f_{in}+f$, the 3×3 matrix [S3] in Fig. 2 can be reduced to a 2×2 matrix [S2] [36]–[37]. Three different 2×2 matrixes can be defined. The first matrix is $S_{b,u}(\Gamma_l^*)$, at the virtual ports at f_b and f_u, depending on $\Gamma_{sb} = \Gamma_l^*$. The second matrix is $S_{b,l}(\Gamma_u)$, at the virtual ports f_b and f_l^*, depending on $\Gamma_{sb} = \Gamma_u$. The third matrix is $S_{l,u}(\Gamma_b)$, at the virtual ports f_l^* and f_u, depending on $\Gamma_{sb} = \Gamma_b$. Using (2), the matrix $S_{b,u}(\Gamma_l^*)$ is obtained as:

$$
\begin{aligned}
s_{bb,r}(\Gamma_o, f, \Gamma_l^*) &= s_{bb} + s_{bl}s_{lb}/(\Gamma_l^{*-1} - s_{ll}) \\
s_{bu,r}(\Gamma_o, f, \Gamma_l^*) &= s_{bu} + s_{bl}s_{lu}/(\Gamma_l^{*-1} - s_{ll}) \\
s_{ub,r}(\Gamma_o, f, \Gamma_l^*) &= s_{ub} + s_{ul}s_{lb}/(\Gamma_l^{*-1} - s_{ll}) \\
s_{uu,r}(\Gamma_o, f, \Gamma_l^*) &= s_{uu} + s_{ul}s_{lu}/(\Gamma_l^{*-1} - s_{ll})
\end{aligned}
\qquad (3)
$$

where the subindex *r* stands for reduced matrix. An analogous calculation is carried out for the other two matrixes $S_{b,l}(\Gamma_u)$ and $S_{l,u}(\Gamma_b)$. For each of the three 2x2 matrixes, six large-signal equivalents of the μ factor [38] can be defined. This will be done using the same expressions as in [38], but considering, in each case, the two virtual ports of the reduced matrix instead of the two physical ports 1 and 2.

The factors $\mu_{b,u}(\Gamma_l^*)$ and $\mu'_{b,u}(\Gamma_l^*)$, calculated from $S_{b,u}(\Gamma_l^*)$, respectively provide the distance to the stability circle in the Γ_b and Γ_u planes at each Γ_l^* value. Analogous factors $\mu_{b,l}(\Gamma_u)$ and $\mu'_{b,l}(\Gamma_u)$, calculated from $S_{b,l}(\Gamma_u)$, and $\mu_{l,u}(\Gamma_b)$ and $\mu'_{l,u}(\Gamma_b)$, calculated from $S_{l,u}(\Gamma_b)$, will also be considered. In each case, the μ and μ' factors provide the same stability information. Thus, the conditional stability analysis can be carried out in terms of three factors: $\mu_{b,u}(\Gamma_l^*)$, $\mu_{b,l}(\Gamma_u)$ and $\mu_{l,u}(\Gamma_b)$, globally denoted as μ_{LS} factors. This three-sideband analysis is demanding since each μ_{LS} factor depends on Γ_{sb} (agreeing in each case with the reflection coefficient inside the parentheses), together with Γ_o and the perturbation frequency *f*. Due to this complexity, the three-band analysis was used in [11] only for validation purposes, under two specific Γ_o values. In the following, the properties of matrix (2) and the three μ_{LS} factors will be studied in order to simplify the analysis methodology.

A. *Consideration of all possible passive values of* Γ_{sb}

Let any of the three factors $\mu_{b,u}(\Gamma_l^*)$, $\mu_{b,l}(\Gamma_u)$ and $\mu_{l,u}(\Gamma_b)$ be considered, which for simplicity will be denoted $\mu_{1,2}(\Gamma_3)$, where 1, 2 and 3 may correspond to any of the three sidebands $f, -f_{in}+f, f_{in}+f$. The terminations at Port 1, Port 2 and Port 3 will be denoted as Γ_1, Γ_2 and Γ_3, respectively. A potentially unstable case will be assumed. By definition, $\mu_{1,2}(\Gamma_3)$ corresponds to the distance from the centre of the Smith chart Γ_2 to the stability circle, which must be evaluated for all the passive values of Γ_3. Let the set of Γ_3 values providing $\mu_{1,2}(\Gamma_3) < 1$ be denoted as Γ_3^U. Then, for any $\Gamma_{3,x} \in \Gamma_3^U$, there will be a set of Γ_2 loads, denoted by $\Gamma_2^U(\Gamma_{3,x})$, such that for any $\Gamma_{2,x} \in \Gamma_2^U(\Gamma_{3,x})$ the input reflection coefficient when looking into Port 1, Γ_{in_1}, fulfils $|\Gamma_{in\_1}(\Gamma_{2,x}, \Gamma_{3,x})| > 1$. The set $\Gamma_2^U(\Gamma_{3,x})$, which will include passive loads, is delimited by a stability circle in Γ_2, expressed as $C_2(\Gamma_{3,x})$.

Now a reduction of the 3×3 scattering matrix to Port 1 and Port 3, depending on Γ_2, will be considered, performing the analysis in terms of the factor $\mu_{1,3}(\Gamma_2)$. Because the first analysis port (Port 1) is the same as in the previous case, for any load $\Gamma_{2,x} \in \Gamma_2^U(\Gamma_{3,x})$ connected to Port 2 and $\Gamma_{3,x}$ connected to Port 3 we will have $|\Gamma_{in\_1}| > 1$. Thus, condition $\mu_{1,3}(\Gamma_2) < 1$ must be fulfilled for any pair of loads $\Gamma_2 \in \Gamma_2^U(\Gamma_{3,x})$, $\Gamma_3 = \Gamma_{3,x}$

. Therefore, if there are Γ_3 values such that $\mu_{1,2}(\Gamma_3)<1$, there must be Γ_2 values such that $\mu_{1,3}(\Gamma_2)<1$.

Next, the connection of a passive load $\Gamma_{1,x}=\left[\Gamma_{in\_1}(\Gamma_{2,x},\Gamma_{3,x})\right]^{-1}$ to Port 1, where $\Gamma_{2,x}\in\Gamma_2^{U}(\Gamma_{3,x})$, and the load $\Gamma_{2,x}$ to Port 2 will be assumed. By Kirchoff's laws, the reflection coefficient when looking into Port 3 will necessarily fulfil $|\Gamma_{in\_3}|>1$. In an analogous manner, when connecting the passive loads $\Gamma_{1,x}$ to Port 1 and $\Gamma_{3,x}$ to Port 3, the reflection coefficient when looking into the Port 2 will fulfil $|\Gamma_{in\_2}|>1$.

One can conclude that if any of the factors $\mu_{b,u}(\Gamma_l^*)$, $\mu_{b,l}(\Gamma_u)$ and $\mu_{l,u}(\Gamma_b)$ is smaller than one for some passive values of the reflection coefficient within the brackets, the other two will also be smaller than one for certain passive values of the reflection coefficient on which they depend. Therefore, to determine whether the amplifier is potentially unstable under mismatch effects it will be sufficient to evaluate exhaustively one of the μ_{LS} factors for all the possible passive values of its corresponding Γ_{sb}.

B. Relationship between the three μ_{LS} factors at the passivity boundary

Let particular terminations at the two sidebands $f_l^*=-f_{in}+f$, $f_u=f_{in}+f$, given by Γ_l^*,Γ_u, be assumed. Then, it will be possible to write:

$$\Gamma_l^*=a_l^*/b_l^*\ ;\ \Gamma_u=a_u/b_u \qquad (4)$$

The above relationships can be combined with (2) to obtain the input reflection coefficient Γ_{in_b} at the baseband, given by $\Gamma_{in\_b}=b_b/a_b$. This provides the following expression, depending on Γ_l^*, Γ_u and the scattering parameters:

$$\Gamma_{in\_b}=\frac{s_{bl}s_{lb}\Gamma_l^*+s_{bu}s_{ub}\Gamma_u+P\,\Gamma_l^*\,\Gamma_u}{1-s_{uu}\Gamma_u-s_{ll}\Gamma_l^*+Q\,\Gamma_l^*\,\Gamma_u} \qquad (5)$$

where the parameters *P* and *Q*, depending only on the scattering parameters, are given by:

$$\begin{aligned} P &= s_{bu}(s_{ub}s_{lu}-s_{lb}s_{uu})+s_{bu}(s_{lb}s_{ul}-s_{ub}s_{ll}) \\ Q &= s_{bb}s_{uu}-s_{lu}s_{ul} \end{aligned} \qquad (6)$$

The amplifier will be unconditionally stable under mismatch effects if $|\Gamma_{in\_b}|<1$ for any pair of values of Γ_l^* and Γ_u, fulfilling $|\Gamma_l^*|\le 1$ and $|\Gamma_u|\le 1$. For notation simplicity, the circles delimiting the passivity boundaries in each of the two planes will be denoted $|\Gamma_l^*|=1$ and $|\Gamma_u|=1$.To determine the images of the passive regions $|\Gamma_l^*|\le 1$ and $|\Gamma_u|\le 1$, one can take into account that for each constant value of Γ_l^*, equation (5) defines a bilinear transformation [17] in the other parameter Γ_u. In an analogous way, for each constant value of Γ_u, equation (5) defines a bilinear transformation in the other parameter Γ_l^*. Thus, the image of the circle $|\Gamma_u|=1$, given by $\Gamma_{in\_b}(|\Gamma_u|=1)$, will be the boundary of the images of all the passive loads $|\Gamma_u|<1$, so all the images $\Gamma_{in\_b}(|\Gamma_u|<1)$ are either inside or outside the transformed circle $\Gamma_{in\_b}(|\Gamma_u|=1)$. The same applies for the bilinear transformation in terms of Γ_l^*, depending on Γ_u.

Applying a similar reasoning, the images of the two circles $|\Gamma_{in\_b}|=1$ and $|\Gamma_l^*|=1$ in the Γ_u plane, obtained through (5), form a global boundary of the images of all the possible passive combinations of Γ_{in_b} and Γ_l^*. This can be rigorously demonstrated as follows. First, let us consider all the pairs Γ_l^*,Γ_u fulfilling:

$$\Gamma_{in\_b}(\Gamma_l^*,\Gamma_u)=1e^{j\varphi} \qquad (7)$$

where $\Gamma_{in\_b}(\Gamma_u,\Gamma_l^*)$ is given by equation (5). Solving for Γ_u one obtains the function:

$$\Gamma_u=\Gamma_u(\Gamma_l^*,\varphi) \qquad (8)$$

Now the following set *L* will be defined:

$$L=\Gamma_u(\Gamma_l^*,\varphi)\ ,\ \forall\varphi,\ \text{such that}\ |\Gamma_l^*|\le 1 \qquad (9)$$

The above mapping can give rise to Γ_u values fulfilling either $|\Gamma_u|<1$ or $|\Gamma_u|>1$. In particular, application of the mapping to the passivity boundary $\Gamma_l^*=1e^{j\phi},\forall\phi\in[0,2\pi]$, denoted as $|\Gamma_l^*|=1$, will provide a set of circles C_u (see Fig. 5), depending on the phase φ:

$$C_u(\varphi)=\Gamma_u(|\Gamma_l^*|=1,\varphi) \qquad (10)$$

For each φ, the whole region $|\Gamma_l^*|<1$ is mapped either inside or outside the circle $C_u(\varphi)$, which constitutes a frontier between points Γ_u belonging or not to the set L for that φ value. When performing this operation $\forall\varphi\in[0,2\pi]$, the boundary of the region *L* is constituted by points belonging to the C_u circles. These points will agree with those in the whole set of stability circles traced in the Γ_u plane for $\Gamma_l^*=1e^{j\phi}$, $\forall\phi\in[0,2\pi]$. The factor $\mu_{b,u}(\Gamma_l^*)$ provides the distance [28] to the stability circle in the Γ_u plane for each Γ_l^*. Because the set of circles $C_u(\varphi)$, $\forall\varphi\in[0,2\pi]$ constitutes the boundary of the Γ_u points such that $|\Gamma_l^*|\le 1$, it will be sufficient to evaluate the factor $\mu_{b,u}(\Gamma_l^*)$ through the circle $\Gamma_l^*=1e^{j\phi}$ to determine the potential instability properties. In fact, a relevant function will be the one providing the minimum value of $\mu_{b,u}(\Gamma_l^*)$ when evaluated through $\Gamma_l^*=1e^{j\phi}$. The resulting value will be denoted as $\mu_u=\min_\phi[\mu_{b,u}(1e^{j\phi})]$.

From the analysis of the mapping in (8), when evaluating $\mu_{b,u}(\Gamma_l^*)$ through a circle $\Gamma_l^*=\rho_o e^{j\phi}$, where $\rho_o<1$, the minimum $\min_\phi[\mu_{b,u}(\rho_o e^{j\phi})]$ will be larger than μ_u and smaller than the one obtained for any other magnitude $\rho<\rho_o$. However, when using $\rho_o<1$ instead of the passivity boundary

$\rho_o = 1$, one must be aware that the three μ_{LS} factors will provide different potential stability predictions, as the analysis is not exhaustive and the evaluation of each of the three μ_{LS} factors will leave out some regions of $|\Gamma_b| \le 1$, $|\Gamma_l^*| \le 1$ and $|\Gamma_u| \le 1$.

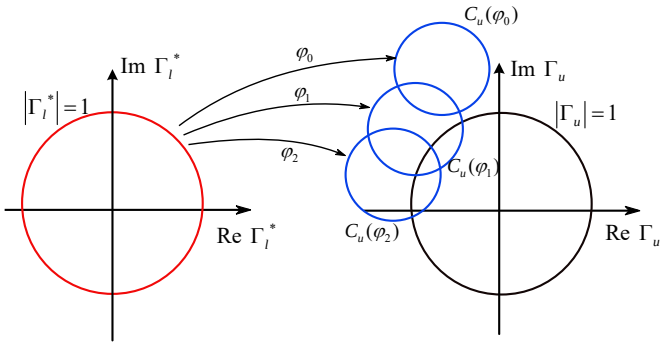

Fig. 5 Formation of the limit set *L* in the Γ_l plane.

For the potential stability analysis, the three parameters $\mu_u = \min_\phi[\mu_{b,u}(1e^{j\phi})]$, $\mu_l = \min_\phi[\mu_{b,l}(1e^{j\phi})]$ and $\mu_u = \min_\phi[\mu_{l,u}(1e^{j\phi})]$ will be initially considered, where it has been taken into account that (in agreement with the properties discussed in subsections *A* and *B*) the minima resulting from $\mu_{b,u}(1e^{j\phi})$ and $\mu_{l,u}(1e^{j\phi})$ should be identical, although obtained for a different phase ϕ in each case. The parameters μ_l and μ_u respectively agree with the minimum distance to the stability circle in the Γ_l^* and Γ_u planes under phase variations in $\Gamma_{sb} = 1e^{j\phi}$. In order to obtain the minimum distance to the stability circle in the Γ_b plane, the parameter $\mu_b = \min[\mu'_{b,l}(1e^{j\phi})]$, agreeing with $\min[\mu'_{b,u}(1e^{j\phi})]$, must also be considered. Note that μ' factors provide the distance to the stability circle in Smith chart corresponding to the "source" termination.

The analysis of the three parameters μ_b, μ_l and μ_u has been applied to the PA in Fig. 1 operating at 0.8 GHz. In an initial study, a Γ_o load describing a spiral curve, $\Gamma_o(h)$, has been considered. The analysis procedure is as follows. At each Γ_o and for each perturbation frequency *f*, the phase ϕ of the reflection coefficient $\Gamma_{sb} = 1e^{j\phi}$ is swept from 0º to 360º, in a fine step, evaluating the factors $\mu'_{b,l}(1e^{j\phi})$, $\mu_{b,l}(1e^{j\phi})$ $\mu_{b,u}(1e^{j\phi})$ and $\mu_{l,u}(1e^{j\phi})$ at each step. Note that $N = 7$ harmonic components are taken into account in the calculation of the 3×3 scattering matrix that enables the determination of these factors. This is the number *N* considered for all the analyses presented in this work. For each *f*, only the minimum values versus ϕ are kept, agreeing with the parameters $\mu_b(f)$, $\mu_l(f)$ and $\mu_u(f)$, where the frequency dependence of these parameters is indicated explicitly. The results obtained for four particular Γ_o values in the spiral curve are shown in Fig. 6. As expected, the minima of $\mu_{b,u}(1e^{j\phi})$ and $\mu_{l,u}(1e^{j\phi})$ are overlapped for all the *f* values.

The three parameters $\mu_b(f)$, $\mu_l(f)$ and $\mu_u(f)$ provide the same information on the potential instability of the PA, in agreement with the derivations in subsections *A* and *B*. Indeed, the three parameters are either larger or smaller than 1 in the same intervals of perturbation frequency *f*. They cross unity at exactly the same frequency values [see the expanded view in Fig. 6(d)].

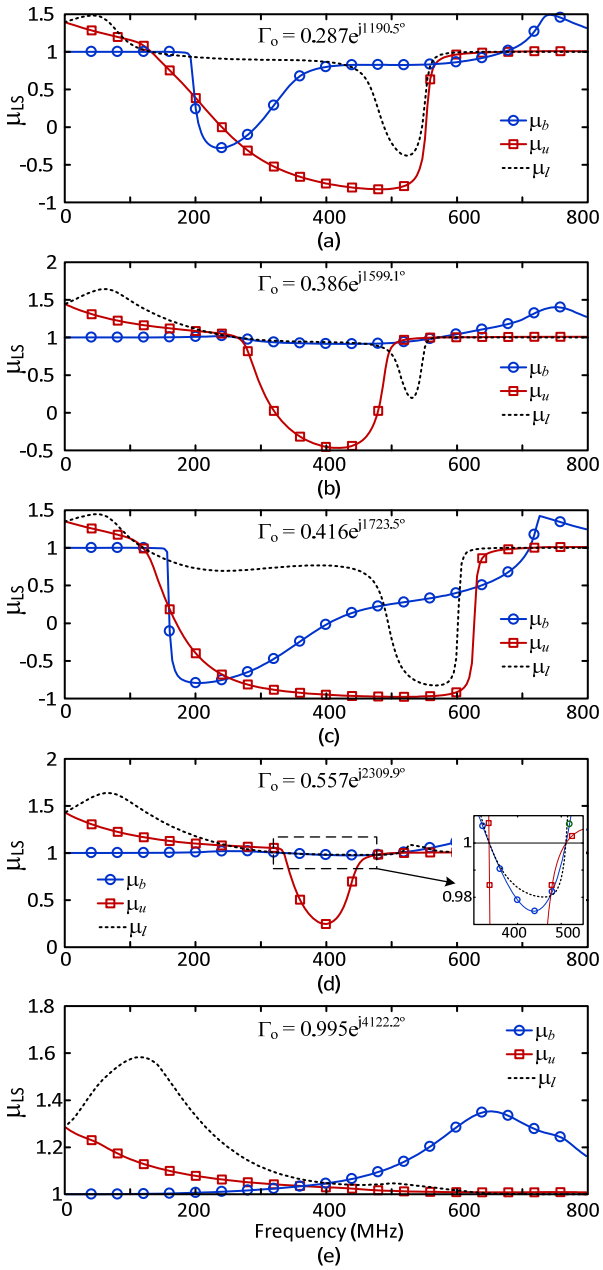

Fig. 6 Variation versus the perturbation frequency *f* the minima of the three factors $\mu_{b,u}(\phi)$, $\mu_{b,l}(\phi)$ and $\mu_{l,u}(\phi)$ with $|\Gamma_{sb}| = 1$, for five particular values of Γ_o. The number of harmonic components considered is $N = 7$. (a) $\Gamma_o = 0.287e^{j110.5°}$, (b) $\Gamma_o = 0.386e^{j159°}$, (c) $\Gamma_o = 0.416e^{j283.5°}$, (d) $\Gamma_o = 0.557e^{j150°}$, and (e) $\Gamma_o = 0.995e^{j162°}$. An expanded view is shown in Fig. 6(d) to show the simultaneous crossing through 1.

For illustration, Fig. 7 presents the values taken by the parameter $\min_{\phi}[\mu_{b,l}(\rho_o e^{j\phi})]$ versus the perturbation frequency f, for ρ_o going from 0 to 1, in steps of 0.1. The termination considered at the fundamental frequency is $\Gamma_o = 0.416e^{j283.5°}$, in Fig. 6(c). As can be seen, the parameter μ_l, agreeing with $\min_{\phi}[\mu_{b,l}(1e^{j\phi})]$ provides the minimum value at each f. Identical results are obtained when analyzing the other two factors $\mu_{b,u}(\Gamma_l^*)$ and $\mu_{l,u}(\Gamma_b)$.

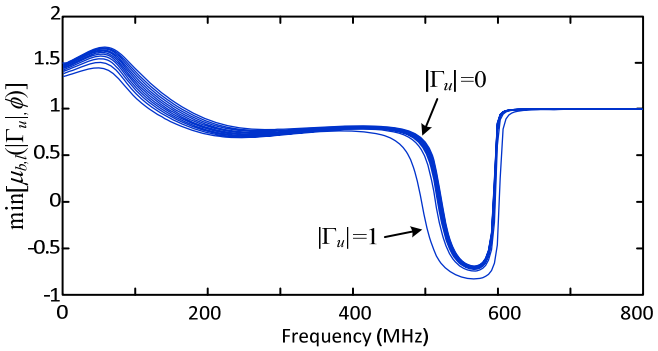

Fig. 7 Frequency variation of the parameter $\min_{\phi}[\mu_{b,l}(\rho_o e^{j\phi})]$ for ρ_o going from 0 to 1, in steps of 0.1. The termination considered at the fundamental frequency is $\Gamma_o = 0.416e^{j283.5°}$, in Fig. 6(c). The number of harmonic components is $N = 7$. The parameter μ_l, agreeing with $\min_{\phi}[\mu_{b,l}(1e^{j\phi})]$ provides the minimum $\mu_{b,l}(\Gamma_u)$ at each f.

C. *Frequency variation of the parameters* μ_b, μ_l and μ_u

For the stability analysis of a periodic regime at f_{in} one should consider variations in the perturbation frequency f between 0 and a value larger than $f_{in}/2$, to enable the detection of frequency divisions by 2. In Fig. 6, the parameters μ_b, μ_l and μ_u have been evaluated in the whole frequency range 0 to f_{in}. The frequency f is an offset with respect to dc, $-f_{in}$ and f_{in}. Therefore, the information obtained for the higher frequency values should be redundant. Indeed, when increasing f, the parameter μ_l provides an "image" of the predictions by the parameter μ_b at lower frequencies. This is very clear in the analyses of Fig. 6(a) and Fig. 6(c).

The frequency variation observed in Fig. 6 is in agreement with the stability properties of periodic solutions. In fact, the poles of periodic solutions, agreeing with the Floquet exponents, are not univocally related to the Floquet multipliers, which do define the stability properties of periodic solutions in a unique manner [29]–[31]. Equivalent poles, associated with the same pair of complex-conjugate Floquet multipliers, are symmetrically located about the spectral lines of the harmonic frequencies of the original periodic regime $k2\pi f_{in}$, that is, they are distributed as $\sigma \pm j(2\pi f + k2\pi f_{in})$. Therefore, the two bands with $\mu_{LS} < 1$ observed in the analysis in Fig. 6 are linked and correspond to the same potential instability, at f and $f_{in} - f$.

Note that the poles at f and $f_{in} - f$ are symmetrically located about $f_{in}/2$, and may tend to this value under variation of a circuit parameter [26], [41]. From Fig. 6, one can expect potential frequency divisions by 2 when the fundamental frequency is terminated at the Γ_o values considered in Fig. 6(a) to Fig. 6(d). However, the region of subharmonic impedances leading to this division is expected to be small, since the values of μ_b and μ_l are close to 1.

The potential frequency division by two predicted in Fig. 6 has been validated with an independent simulation. A small signal current source at $f_{in}/2$ is introduced into the circuit at the output reference plane [Fig. 8(a)]. At f_{in}, the circuit is loaded, in each case, with one of the Γ_o values considered in Fig. 6. Instead of using a modified conversion-matrix approach as in [33], [42], a harmonic balance analysis at $f_{in}/2$ is carried out. It is taken into account that there must be a phase relationship between the subharmonic current source and the input generator, due to the coherency of the two signals. The phase of the subharmonic source is set to zero (phase origin). Then, the phase of the input source ϕ_{in} is swept, using the small-signal current source to calculate the input admittance at the subharmonic component $Y_{in}(f_{in}/2, \phi_{in})$ at each phase step. The opposite admittance values $Y_{Lb}(\phi_{in}) = -Y_{in}(f_{in}/2, \phi_{in})$ fulfill a limit condition for frequency division by 2, with subharmonic amplitude tending to zero, and provide the boundary in the Smith chart corresponding to the subharmonic load. The points of this boundary correspond to flip bifurcations [26], [41]. To obtain the frequency-division boundary in the Smith chart at $f_{in}/2$, the reflection coefficient associated to $Y_{Lb}(\phi_{in})$ must be calculated.

The above method has been applied for the Γ_o values considered in Fig. 6(b), (d) and (e), corresponding to $\Gamma_o(b) = 0.39e^{j159°}$, $\Gamma_o(d) = 0.56e^{j150°}$ and $\Gamma_o(e) = 0.995e^{j162°}$. The division boundary, obtained with the technique in Fig. 8(a), has been traced in Fig. 8(b) for the three cases. It only intersects the Smith chart for $\Gamma_o(b)$ and $\Gamma_o(d)$. The passive $f_{in}/2$ loads enabling the frequency division are inside the division boundary. This division region is small, in agreement with the quantitative predictions of Fig. 6. This correspondence is found, despite the fact that the two types of analysis are fundamentally different, since the subharmonic current source in Fig. 8(a) has a phase relationship with the input generator.

The capability to obtain frequency divisions for passive loads within the boundaries obtained in Fig. 8(a) has also been validated with an independent HB simulation. For the subharmoinc load $\Gamma_L(f_{in}/2) = 0.993e^{-j294.4°}$ and $\Gamma_o(f_{in}) = 0.386e^{j159°}$, one obtains the spectrum of Fig. 8(c).

The results of the three-band analysis have been compared in Fig. 9 with that obtained when using the single μ_{LS} factor considered in [11], for which the analysis is restricted to the lower and upper sidebands f_l^* and f_u. This two-band μ_{LS} factor should agree with the one obtained with $\mu_{l,u}(\Gamma_b)$, when imposing a particular termination at baseband, such as $\Gamma_b = 0$,

which was considered in [11] and also here. Therefore, it has more limited prediction capabilities. As an example, in Fig. 9, corresponding to the fundamental-frequency termination $\Gamma_o(f_{in}) = 0.557e^{j150^\circ}$ in Fig. 6(d), the two-sideband method predicts stable behaviour, whereas the three-sideband one predicts potential instability.

To extend the method to mismatch effects at higher harmonic terms one should consider all possible sets of harmonic impedance terminations, and obtain an M-port scattering matrix for each combination of harmonic impedances, where *M* is the total number of mismatched sidebands. All the μ_{LS} factors defined between any two ports of the M-port scattering matrix will provide the same information on the potential instability, under the condition that the reflection coefficients of the termination loads at all the other ports describe a unit circle. Such computational effort will not be worth in most cases due to the filtering action of the output network.

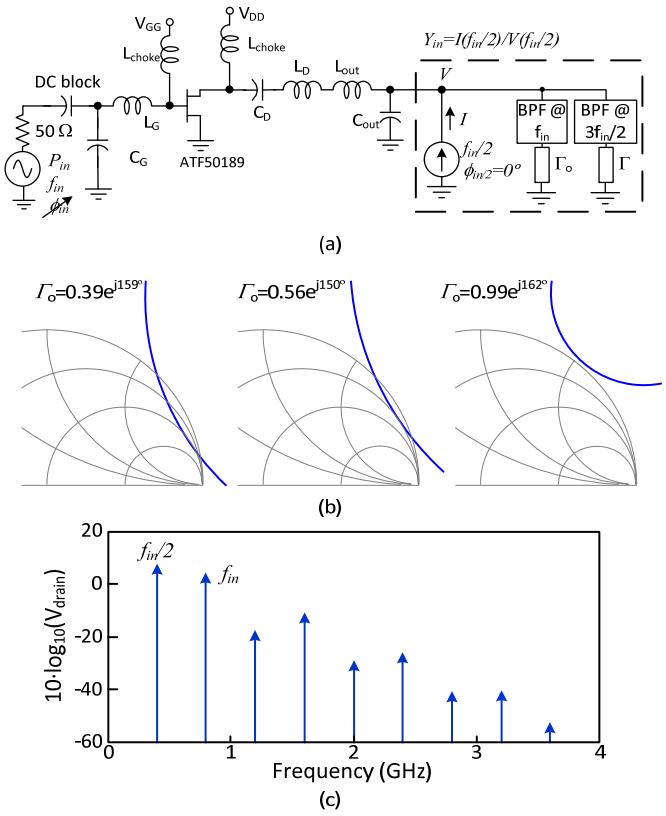

Fig. 8 Validation of the capability to predict frequency divisions by 2. (a) Independent simulations using a small-signal current source at $f_{in}/2$ (b) Boundaries of passive loads at the subharmonic frequency giving rise to frequency divisions for three Γ_o values considered in Fig. 6. (c) Spectrum of the subharmonic solution obtained with an independent HB simulation for $\Gamma_L(f_{in}/2) = 0.993e^{-j294.4^\circ}$ and $\Gamma_o = 0.386e^{j159^\circ}$.

The three-sideband stability analysis will be validated with measurements, in Section V, and with independent simulations through pole-zero identification, in the next section. Verification through simulation enables a high accuracy, under the certainty that the passive and active component models are identical. This validation will rely on the calculation of stability circles in the plane corresponding to the baseband termination Γ_b. The predictions obtained with these circles will be compared with the results of an accurate pole-zero identification at circuit level [15], [28], [39].

IV. Stability Circles in the Three-Sideband Analysis

In this section, the use of stability circles when considering three sideband frequency terminations (besides the fundamental-frequency termination Γ_o) is presented and applied for an independent validation of the new outer-tier methodology. Selecting particular sets of values $\Gamma_b, \Gamma_l^*, \Gamma_o, \Gamma_u$ with different stability properties would require a demanding implementation of a frequency dependent load $\Gamma_L(f)$, exhibiting the values $\Gamma_b, \Gamma_l^*, \Gamma_o, \Gamma_u$ at the corresponding frequencies. Instead, a simple passive network will be considered here, which under modification of an element value should give rise to different stability conditions of the PA. Next, the values exhibited by the load at the four frequencies f_b, f_l^*, f_{in}, f_u will be calculated to check the consistency with the potential instability analysis.

The load will consist of an inductor *L* in series with a resistor *R*, which fits commonly used antenna models. When connected to the amplifier output (replacing the nominal 50 Ω load) and under variations of the inductor *L*, at constant *R* = 5 Ω, it gives rise to different stability conditions, as predicted by the pole-zero identification method. Fig. 10 presents the variation of the real part of the dominant pair of complex-conjugate poles versus the inductor *L*, at constant input power P_{in} = 12 dBm. As gathered from Fig. 10, the PA is stable for $L < 10.69$ nH, and unstable for $L \geq 10.69$ nH. The circuit exhibits a Hopf bifurcation at the inductor value L_{c1} = 10.69 nH.

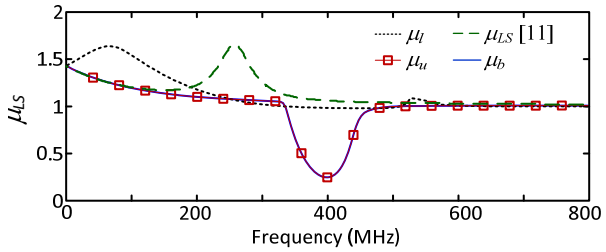

Fig. 9 Comparison of the results obtained with the new potential-stability analysis, using the three factors μ_b, μ_l and μ_u, with those obtained using the single μ_{LS} factor considered in [11].

The first validation will be carried out at the Hopf bifurcation point obtained for L_{c1} = 10.69 nH. The poles crossing the imaginary axis have the critical frequency f_c = 204.595 MHz, as obtained from the pole-zero identification. At the baseband, lower sideband, fundamental and upper sideband frequencies given by $f_{b,c} = f_c$ = 204.595 MHz, f_{in} = 0.8 GHz, $f_{in} - f_c$ and

$f_{in} + f_c$, the R–L load exhibits the reflection coefficients shown in Table I.

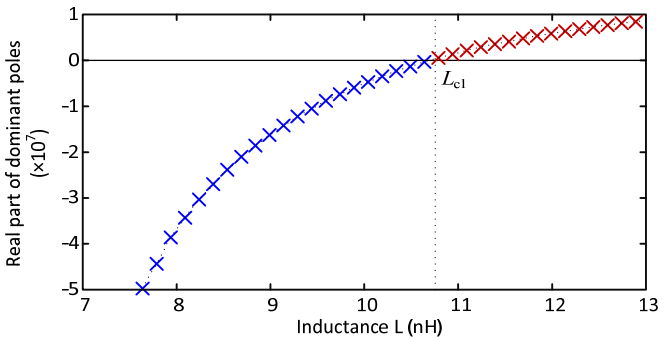

Fig. 10 Variation of the real part of the dominant pair of complex-conjugate poles versus the inductor L, with R = 5 Ω, at constant input power P_{in} = 12 dBm.

TABLE I
REFLECTION COEFFICIENT OF THE R-L LOAD AT THE BIFURCATION POINT

	Frequency (MHz)	Γ
Γ_b	204.595	$0.82998 \cdot e^{j148.9°}$
Γ_l	595.405	$0.88534 \cdot e^{j102.3°}$
Γ_o	800.000	$0.91156 \cdot e^{j85.58°}$
Γ_u	1004.59	$0.93173 \cdot e^{j72.86°}$

Next, the [S_3] outer-tier matrix in (2) will be used to obtain the stability circles in the Γ_b Smith chart, when the perturbation frequency f varies in the interval from f_1 =30 MHz to f_2 = 370 MHz about the critical value $f_{b,c}$ = 204.595 MHz. At the fundamental frequency f_{in} = 0.8 GHz, the load exhibits the reflection coefficient $\Gamma_o = 0.91156 e^{j85.58°}$. For this particular Γ_o, the stability circles will be obtained reducing the [S_3] matrix to a 2×2 matrix at the sideband frequencies f and $f_{in} + f$, depending on the termination $\Gamma_l^*(f)$. This reduced matrix will be expressed as $S_{bu}\left(f, \Gamma_l^*(f)\right)$. At each f the 2×2 matrix is calculated for the precise $\Gamma_l^*(f)$ value exhibited by the series R-L load at $-f_{in} + f$.

The stability circles obtained from the matrix $S_{bu}\left(f, \Gamma_l^*(f)\right)$ are traced in the plane Γ_b, for perturbation frequencies from f_1 to f_2 [Fig. 11(a)]. For perturbation frequencies such that $|s_{uu,r}| < 1$, the stability circle is traced in solid line. When $|s_{uu,r}| > 1$, the circle is traced in a dashed line. This allows distinguishing between the potentially unstable and stable regions. The circle obtained for the critical perturbation frequency $f_{b,c}$ = 204.595MHz is traced in a bolder line. The variation of the reflection coefficient exhibited by the series R-L load $\Gamma_L(f)$ through the interval f_1 to f_2 has also been represented. Around the critical frequency f_c, the load values $\Gamma_L(f)$ are located, as expected, in the potentially unstable region.

Next, the bifurcation condition at $f_{b,c}$ = 204.595 MHz will be validated. At this frequency, the R–L load exhibits the coefficient $\Gamma_l^* = \Gamma_L(-f_{in} + f_{b,c}) = 0.88534 e^{-j102.3°}$, shown in Table I. Setting the reflection coefficient at the baseband frequency to $\Gamma_b = 0.82998 e^{j148.9°}$ and using the matrix $S_{bu}\left(f, \Gamma_l^*(f)\right)$ one obtains at the upper sideband frequency $f_{in} + f_{b,c}$ the input reflection coefficient $\Gamma_{u\_in} = 1.0743 e^{-j72.85°}$. This value fully agrees with the inverse of the reflection coefficient exhibited by the R–L load at the upper sideband frequency, i.e. $\Gamma_u = 0.93173 e^{j72.85°}$ (see Table I). Thus, the bifurcation condition $\Gamma_{u\_in} / \Gamma_u = 1$ is fulfilled, in total consistency with the results of pole-zero identification.

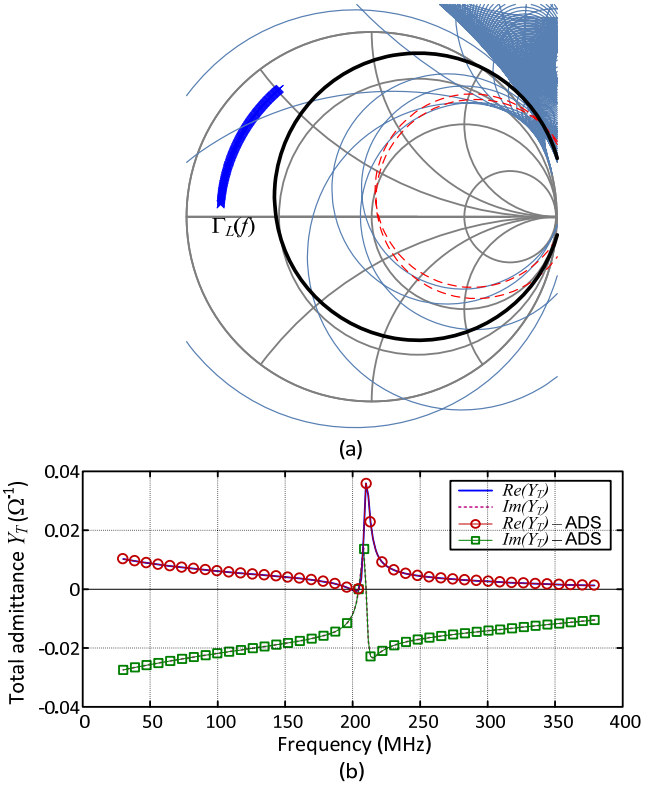

Fig. 11 Stability conditions at L_{c1} = 10.69 nH (bifurcation point in Fig. 10). (a) Stability circles for $\Gamma_o = 0.91156 e^{j85.58°}$ traced in the Γ_b plane for $\Gamma_l^*(f)$ values corresponding to those exhibited by the R-L load in the frequency interval f_1 = 30 MHz to f_2 = 370 MHz about the critical value $f_{b,c}$ = 204.595 MHz. For perturbation frequencies such that $|s_{uu,r}| < 1$ ($|s_{uu,r}| > 1$), the stability circle is traced in solid (dashed) line. The variation of the Γ_b exhibited by the R–L load in the same frequency interval has also been represented. (b) Total admittance function $Y_T(f_{in} + f) = Y_{in\_u} + Y_u$, calculated with the three-sideband outer-tier analysis and with a full conversion-matrix approach in HB, using 7 harmonic terms.

As an additional validation, the total admittance function $Y_T(f_{in} + f) = Y_{in\_u} + Y_u$, calculated with the three-sideband outer-tier analysis has been compared with the one obtained with a full conversion-matrix approach in commercial harmonic balance, using 7 harmonic terms. For the full conversion-matrix approach, a small-signal current source is introduced in parallel with the output R-L load to calculate the total admittance function, as the ratio between the source current and the node voltage. Results are shown in Fig. 11(b). As can be seen, the

curves for both the real and imaginary parts are overlapped and display a bifurcation point at $f_{b,c}$ = 204.595 MHz, where the real and imaginary parts of the total admittance are equal to zero.

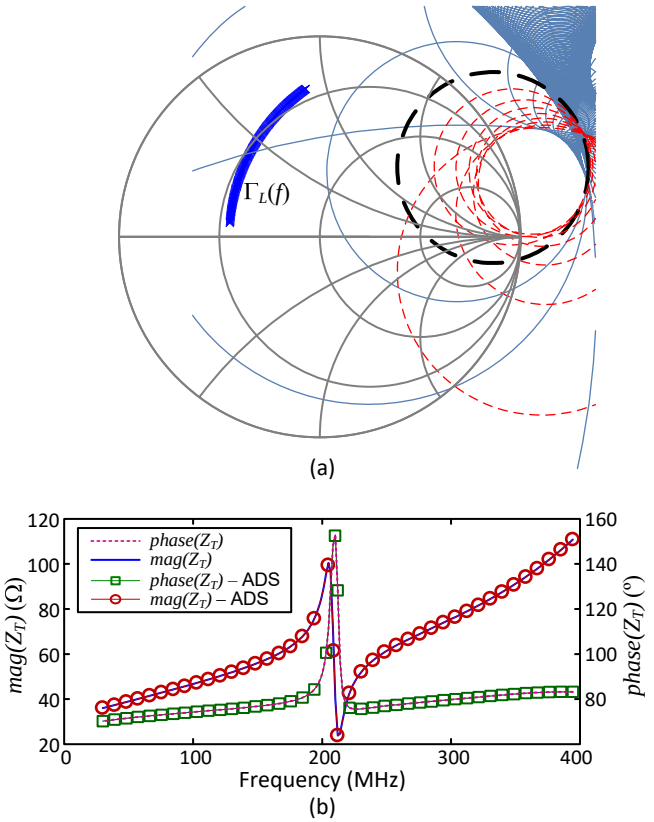

Fig. 12 Stability conditions for L = 11.4 nH. (a) Stability circles for $\Gamma_o = 0.91733e^{j81.97}$ traced in the Γ_b plane for Γ_l^* values corresponding to those exhibited by the R-L load about the frequency of the dominant poles (f_c = 212.176 MHz). For perturbation frequencies such that $|s_{uu,r}|<1$ ($|s_{uu,r}|>1$), the stability circle is traced in solid (dashed) line. The variation of the Γ_b exhibited by the R–L load in that frequency interval has also been represented. (b) Impedance function $Z_T(f) = 1/(Y_{in\_u} + Y_u)$ calculated with the three-sideband outer-tier analysis and with a full conversion-matrix approach in HB, using 7 harmonic terms.

Next, inductor values L in the unstable and stable ranges predicted by the pole-zero identification will be considered. From Fig. 10, for L = 11.4 nH, the amplifier is unstable. The stability circles are calculated for the new reflection coefficient $\Gamma_o = 0.91733e^{j81.97°}$, exhibited by the modified load R = 5 Ω, L = 11.4 nH at f_{in} = 0.8 GHz. They have been traced in the Γ_b Smith chart [Fig. 12(a)] for the Γ_l^* values exhibited by the new R–L load in the perturbation-frequency interval f_1 = 30 MHz to f_2 = 390 MHz, which includes the frequency f_c = 212.176 MHz of the dominant pair of complex-conjugate poles at L = 11.4 nH. The stability circle at f_c has been traced in a bolder line and the unstable region corresponds to the outside of this circle, where the Γ_b exhibited by the R-L load is located. This indicates, as expected, potential instability for this baseband termination. Next, the input admittance at the upper sideband $Y_u(f)$ is calculated using $S_{bu}\left(f, \Gamma_l^*(f)\right)$ and $\Gamma_b(f)$. This allows the evaluation of the impedance-type transfer function $Z_T(f) = 1/(Y_{in\_u} + Y_u)$, analogous to the transfer function usually chosen for pole-zero identification [8], [15] [Fig. 12(b)]. This function has been compared with the one obtained through the full conversion matrix approach in harmonic balance (with 7 harmonic terms), obtaining a full overlap of both the amplitude and phase. The impedance exhibits a clear resonance at the frequency of the dominant poles, with a positive phase slope that indicates unstable behaviour, in total agreement with the pole-zero analysis in Fig. 10.

Next value is L = 10 nH, in the stable region predicted by the pole analysis of Fig. 10. Most of the stability circles obtained under variations of $\Gamma_l^*(f)$ about the frequency of the dominant poles at L = 10 nH, lie outside the Smith chart [Fig. 13(a)]. The circle corresponding to this precise frequency value has been traced in bolder line and indicates absolute stability. The impedance transfer function $Z_T(f) = 1/(Y_{in\_u} + Y_u)$ [shown in Fig. 13(b)], obtained with the three-sideband outer tier analysis, is fully overlapped with the one resulting from a full conversion-matrix approach in HB, using 7 harmonic terms. It has a negative phase slope, in agreement with the stable behaviour predicted by pole-zero identification.

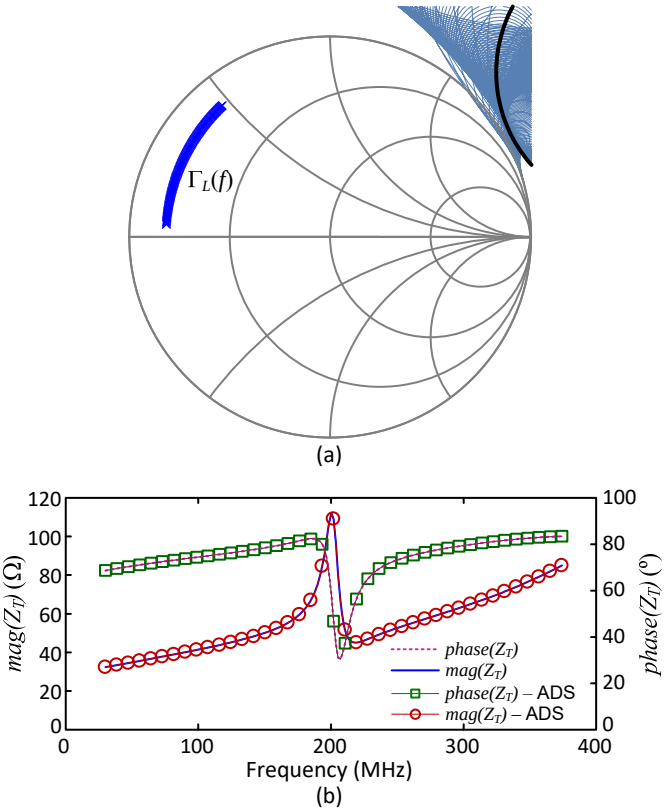

Fig. 13 Stability conditions for L = 10 nH. (a) Stability circles for $\Gamma_o = 0.90547e^{j89.41°}$ traced in the Γ_b plane for Γ_l^* values corresponding to those exhibited by the R-L load in the frequency interval f_1=30 MHz to f_2 = 370 MHz about the frequency of the dominant poles f_c = 202.01 MHz. The variation of the Γ_b exhibited by the R–L load in that frequency interval has also been represented. (b) Impedance function $Z_T(f) = 1/(Y_{in\_u} + Y_u)$ calculated with the three-sideband outer-tier analysis and with a full conversion-matrix approach in HB, using 7 harmonic terms.

V. Definition of a Global Stability Parameter

As has been shown, the potential stability properties exhibit a multi-parameter dependence, changing with the fundamental-frequency termination Γ_o, the perturbation frequency *f* and the terminations at the three sideband frequencies. In view of this complexity, the goal will be the derivation of a single quantity, globally accounting for the stability properties at each fundamental-frequency termination Γ_o. The three parameters $\mu_b(f)$, $\mu_l(f)$ and $\mu_u(f)$, with their crossings through 1, provide the same information regarding the conditional or unconditional stability properties. However, the actual parameter values are interesting since they contain useful information on the stability margin. Indeed, at each perturbation frequency they provide the minimum distance to the stability circles in the respective planes Γ_b, Γ_l^* and Γ_u.

The analysis will be initially particularized to $\mu_b(f)$. In fact, this parameter (as well as the other two parameters μ_l and μ_u) will vary with the perturbation frequency *f* and with the fundamental-frequency termination Γ_o. This is because the scattering matrix in (2) depends on this termination, which affects the steady-state solution about which the circuit is linearized. The double dependence will now be emphasized with the explicit notation $\mu_b(\Gamma_o, f)$. The parameter μ_b (as well as μ_l and μ_u) is continuous in the frequency *f*, due to the continuity of the scattering matrix, as evidenced by the results of Fig. 6. On the other hand, continuity with respect to Γ_o is ensured by the smooth behavior of the set of nonlinear algebraic equations composing the HB system. Taking into account these continuity properties, a global stability parameter, associated with μ_b, may be defined:

$$\mu_b^T(\Gamma_o) = \min_f \left[\mu_b(\Gamma_o, f)\right] \qquad (11)$$

which corresponds to the minimum value taken by $\mu_b(\Gamma_o, f)$ in the perturbation-frequency interval. The above parameter contains the full information on the potential instability conditions at each particular termination Γ_o. Identical parameters $\mu_l^T(\Gamma_o)$ and $\mu_u^T(\Gamma_o)$ can also be defined for the lower and upper sidebands.

To gather the whole information on the impact of the fundamental-frequency termination Γ_o on the potential stability properties, the analysis set-up in Fig. 2(a) must be used. A double sweep must be carried out in the amplitude and phase of Γ_o (or a spiral sweep), performing, at each sweep step, a large-signal small-signal analysis to obtain the impedance matrix [Z_3]. This matrix, depending on both Γ_o and *f*, is transformed to a scattering matrix and exported to in-house software to calculate the parameters $\mu_b^T(\Gamma_o)$, $\mu_l^T(\Gamma_o)$ and $\mu_u^T(\Gamma_o)$. Then, their variation with Γ_o can be evaluated through contour plots traced in the Γ_o Smith chart. When using these single numbers to characterize the potential stability properties, information on the most dangerous perturbation frequencies is lost, but can be easily recovered through inspection of the frequency plots used in Fig. 6, obtained with an undemanding spiral sweep applied to Γ_o, as done in Fig. 6.

The above global analysis has been applied to the modified PA in Fig. 1, at the nominal operation point, with output power P_{out} = 22 dBm and efficiency 80%. Fig. 14 shows the contour plots of $\mu_b^T(\Gamma_o)$ and $\mu_l^T(\Gamma_o)$ in the Γ_o Smith chart. At the limit of potential instability, corresponding to $\mu_b^T(\Gamma_o)$ and $\mu_l^T(\Gamma_o) = 1$, the contours agree in the two cases. When moving rightwards from these two contours, the two parameters decrease continuously from 1, but in a different manner. The parameter $\mu_l^T(\Gamma_o)$ decreases faster than $\mu_b^T(\Gamma_o)$.

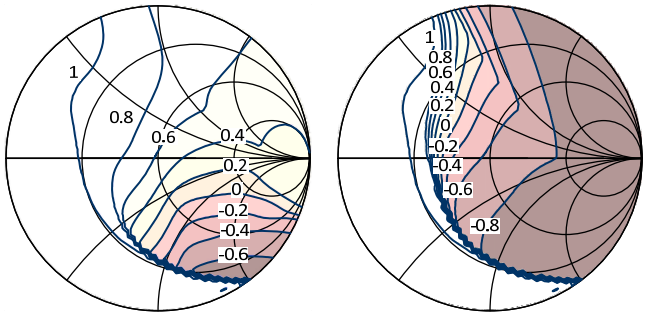

Fig. 14 Contour plots of $\mu_b^T(\Gamma_o)$ and $\mu_l^T(\Gamma_o)$ in the Γ_o Smith chart. The contours at the limit of potential instability, corresponding to $\mu_b^T(\Gamma_o)$ and $\mu_l^T(\Gamma_o) = 1$, agree in the two cases.

The simulations in Fig. 14 have been validated with exhaustive measurements. The measurement test-bench is shown in Fig. 15. Initially, a triple stub tuner has been connected to the PA output. Multiple positions of the tuner have been tested. For each position, both the PA output spectrum and the input impedance exhibited by the tuner about the fundamental frequency f_{in} have been measured. The tuner input impedance has been characterized with a network analyser. These exhaustive tests have provided the results shown in Fig. 16. The impedance plots corresponding to stable behaviour are marked with squares in Fig. 16(a). The corresponding ensemble of output spectra is shown in Fig. 16(b) and evidences stable behaviour in all cases. The impedance plots corresponding to unstable behaviour are marked with circles in Fig. 16(a). The measured output spectrum corresponding to each termination load is shown in Fig. 16(b), in the case of stable loads, and in Fig. 16(c), in the case of unstable loads. These representations allow noting the output-power variation with the termination load. In Fig. 16(d) and Fig. 16(e), the output spectra are projected on the frequency – power plane, which, in the case of the unstable loads evidences undesired spectral components due to the PA self-oscillation.

Very good agreement is found when comparing the experimental results in Fig. 16 with the stability predictions based on the contour plots of $\mu_b^T(\Gamma_o)$ and $\mu_l^T(\Gamma_o)$ in Fig. 14. On the other hand, the oscillation frequency is most usually within the regions of lowest μ_{LS} values detected in Fig. 6. It should be emphasized that the contour plots in Fig. 14

inherently contain the information on the circuit linearized response versus a perturbation at an incommensurate frequency *f*, as gathered from their definition in (11).

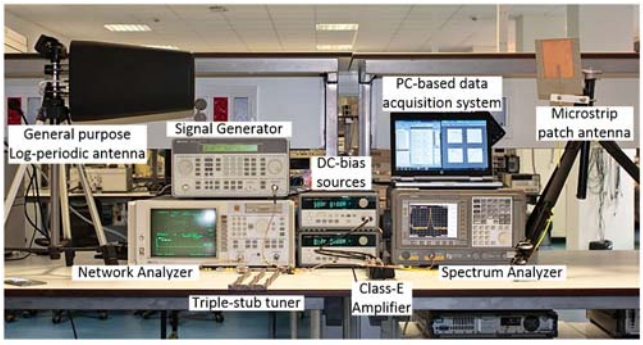

Fig. 15 Measurement test-bench. A triple-stub tuner has been used as output load in the first measurement campaign to identify load values in the stable and unstable regions of the Smith Chart. It was later substituted by a microstrip patch antenna (Rogers 4003C).

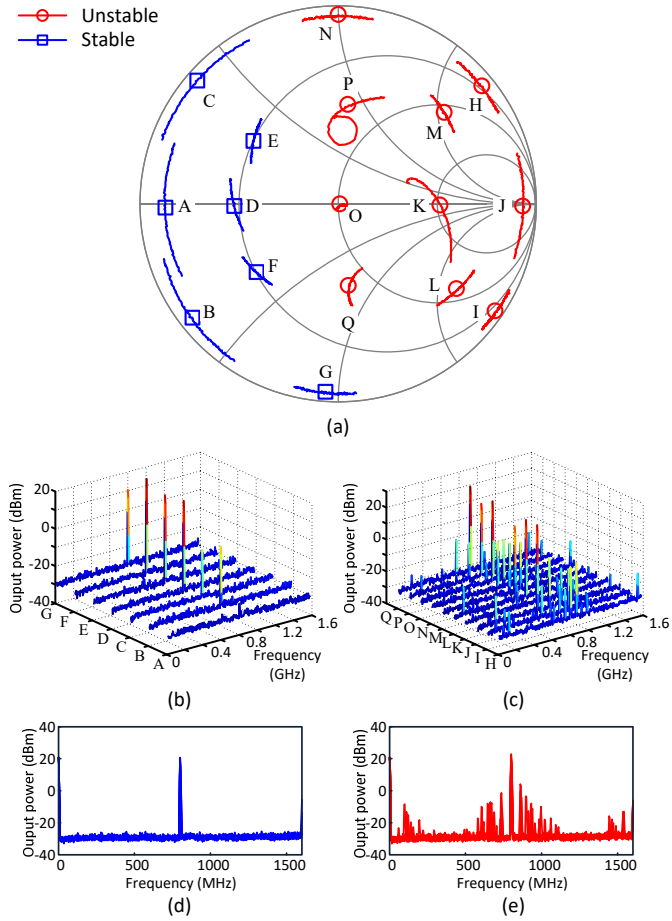

Fig. 16 Exhaustive measurements with a triple stub tuner, where multiple positions of the tuner have been tested. (a) Impedance plots for the different positions of the tuner, corresponding to the curves A to Q, measured in a 40 MHz span. Stable and unstable points are marked with squares and circles, respectively. (b) Waterfall representation of the spectra measured for the stable loads. (c) The same representation for the unstable loads. (d) and (e) Projection of the measured spectra in (b) and (c), respectively.

The results obtained with the contour plots in Fig. 14 and the exhaustive experimental characterization in Fig 16 have also been validated in conditions close to those in real applications.

The PA has been connected to a patch antenna fabricated on Rogers 4003C, shown in Fig. 17(a). The VSWR of the manufactured antenna has been characterized and its lowest value is obtained at 787 MHz, instead of the PA operation frequency 800 MHz [Fig. 17(b)]. Fig. 17(c) shows the variation of its input reflection coefficient in the Smith chart.

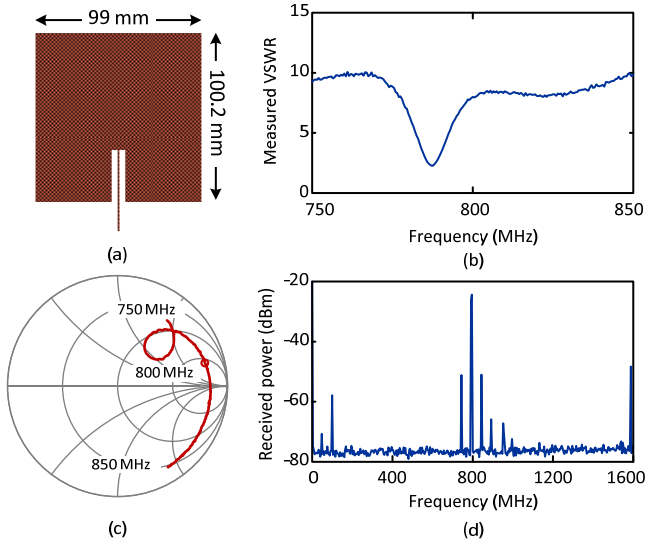

Fig. 17 PA behaviour when connected to a patch antenna. (a) Antenna fabricated on Rogers 4003C (b) Measurement of the antenna VSWR. (c) Measured variation of its input reflection coefficient in the Smith chart. (d) Spectrum received by the log-periodic antenna demonstrating the unstable behaviour of the PA.

For the stability characterization of the PA loaded with the patch antenna, the transmitted signal is received by a general purpose log-periodic broadband antenna, connected to a network analyzer. See the details of the measurement test bench in Fig. 15. By performing the measurement without a directional coupler, power splitter or analogous devices, used to take a sample of the output spectrum, one can be sure that the only loading effects of the PA are those coming from the antenna input impedance.

Taking into account the contour plots in Fig. 14, from a simple inspection of the antenna input impedance in Fig. 17, one can anticipate that the PA loaded with this antenna will be unstable. Indeed, when connecting the antenna to the PA output, an oscillation is obtained, shown in Fig. 17(d).

In the next experiment, a directional coupler will be inserted between the PA output and the antenna. Before that, the input impedance of the subsystem composed by the cascade connection of the directional coupler and the antenna has been measured, obtaining the plot displayed in Fig. 18(a). The measured VSWR is shown in Fig. 18(b). From inspection of the plot in Fig. 18(a), located in the stable region of the Γ_o Smith chart, according to the contour plots in Fig. 14, the PA should be stable. This is confirmed by the spectrum measured in Fig. 18(c), which shows a stable behaviour.

The three-sideband analysis followed by the contour plots provides an easy-to-apply methodology for the detection and suppression of instabilities due to mismatch effects.

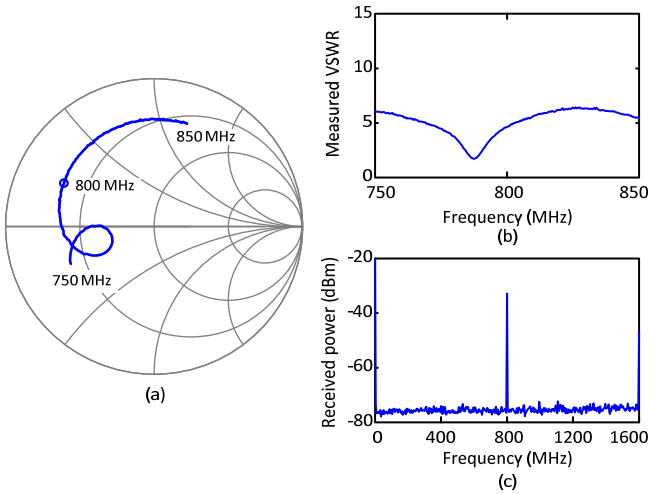

Fig. 18 PA behaviour when a directional coupler is inserted between the PA output and the antenna. (a) Input impedance of the subsystem composed by the cascade connection of the directional coupler and the antenna. (b) Frequency variation of the measured VSWR. (c) Measured spectrum showing a stable behaviour.

VI. Conclusion

A general application method for the prediction of potential instability in power amplifiers under mismatch effects has been presented. It is based on the extraction of an outer-tier scattering matrix at the three sideband frequencies with impact on the stability properties, which in most cases will correspond to the baseband and the lower and upper frequency sidebands. With the inclusion of the baseband, the analysis is more accurate and complete, and enables the prediction of common instabilities, occurring around the input frequency divided by 2. The termination at the fundamental frequency affects the steady-state solution and hence the outer-tier matrix, which is based on a linearization of the circuit about this solution. The complexity associated to the multiparameter dependence is resolved with a detailed analysis of the properties of the three different μ factors that can be associated to the 3×3 matrix. Form these analysis, three new parameters have been defined, able to provide global information on the potential instability properties. Contours plots of these parameters enable a simple identification of the fundamental-frequency terminations leading to potential instability and provide valuable information to devise a stabilization procedure.

References

[1] D. Qiao, D. Cho, Y. Zhao, T. Hung, D. Kimball, M. Li, P. Asbeck, "Antenna impedance mismatch measurement and correction for adaptive CDMA transceivers," *IEEE MTT–S Int. Microwave Symp*, 2005.

[2] A. van Bezooijen, C. Chanlo, A. van Roermund, "Adaptively preserving power amplifier linearity under antenna mismatch," *IEEE MTT–S Int. Microwave Symp*, Fort Worth, pp. 1515–1518, 2004.

[3] A. Keerti, and A. H. Pham, "RF Characterization of SiGe HBT Power Amplifiers Under Load Mismatch", *IEEE Trans. Microw. Theory Techn.*, vol. 55, no. 2, Feb., 2007.

[4] W. Karoui, W. T Parra, "A protection circuit for HBT RF Power Amplifier under load mismatch conditions," *Circuits and Systems and TAISA Conference, Joint 6th International IEEE Northeast Workshop*, pp. 241–244, 22–25 Jun., 2008.

[5] S. Dellier, R. Gourseyrol, J. Collantes, A. Anakabe, G. Soubercaze–Pun, K. Narendra, "Stability analysis of microwave circuits," *(WAMICON), 2012 IEEE 13th Annual* , vol., no., pp.1–5, 15–17 Apr., 2012.

[6] K. Narendra, E. Limiti, C. Paoloni, J. M. Collantes, R. Jansen, and S. Yarman, "Vectorially Combined Distributed Power Amplifiers for Software-Defined Radio Applications," *IEEE Trans. on Microw. Theory and Techn.*, vol. 60, no. 10, Oct., 2012.

[7] J. F. Imbornone, M. Murphy, R .S. Donahue and E. Heaney, "New insight into subharmonic oscillation mode of GaAs power amplifiers Under Severe Output Mismatch Condition," *IEEE Journal of Solid State Circuits*, vol. 32, pp. 1319–1325, Sept., 1997.

[8] A. Anakabe, et al. "Automatic pole–zero identification for multivariable large–signal stability analysis of RF and microwave circuits," *European Microwave Conference (EuMC)*, Paris, pp. 477–480, 2010.

[9] A. Suárez, F. Ramírez, S. Sancho, "Stability analysis of power amplifiers under mismatching effects," *2013 IEEE MTT-S Int. Microwave Symp.*, Seattle, WA, USA, Jun., 2013.

[10] A. Suárez, F. Ramírez, S. Sancho, "Stability Analysis of Power Amplifiers Under Output Mismatch Effects," *IEEE Trans. Microw. Theory Techn.*, vol. 62, no. 10, pp. 2273–2289, Oct., 2014.

[11] A. Suárez, F. Ramírez, S. Sancho, "Stability criteria for power amplifiers under mismatch effects," *2015 IEEE MTT-S Int. Microwave Symp.*, Phoenix, AZ, USA, May, 2015.

[12] V. Rizzoli and A. Neri, "State of the art and present trends in nonlinear microwave CAD techniques," *IEEE Trans. Microw. Theory Techn.,* vol. 36, pp. 343–356, Feb., 1988.

[13] V. Rizzoli, A. Lipparini, "General Stability Analysis of Periodic Steady–State Regimes in Nonlinear Microwave Circuits," *IEEE Trans. Microw. Theory Techn.*, vol. 33, no. 1, 1985, pp. 30–37.

[14] R. Quéré, E. Ngoya, M. Camiade, A. Suarez, M. Hessane and J. Obregon, "Large signal design of broadband monolithic microwave frequency dividers and phase–locked oscillators," *IEEE Trans. Microw. Theory Techn.*, vol. 41, pp. 1928–1938, Nov., 1993.

[15] J. Jugo, J. Portilla, A. Anakabe, A. Suárez, and J. M. Collantes, "Closed–loop stability analysis of microwave amplifiers," *IEE Electronics Letters*, vol. 37, pp. 226–228, Feb., 2001.

[16] N. O. Sokal, A. D. Sokal, "Class E – A New Class of High Efficiency Tuned Single-Ended Switching Power Amplifiers", IEEE Journal of Solid-State Circuits, vol. SC-10, no. 3, pp. 168-176, Jun. 1975.

[17] F. H. Raab, "Idealized Operation of the Class E Tuned Power Amplifier", IEEE Transactions on Circuits and Systems, vol. 24, no. 12, pp. 725-735, December 1977.

[18] K. Chen, D. Peroulis, "Design of Highly Efficient Broadband Class-E Power Amplifier Using Synthesized Low-Pass Matching Networks," *IEEE Transactions on Microwave Theory and Techniques*, vol. 59, no. 12, pp. 3162-3173, Dec. 2011

[19] M. Franco, A. Katz, "Class-E Silicon Carbide VHF Power Amplifier," *IEEE/MTT-S International Microwave Symposium*, 2007, pp. 19-22, 3-8 June 2007.

[20] S. Jeon, A. Suárez, and D.B. Rutledge, "Analysis and elimination of hysteresis and noisy precursors in power amplifiers," *IEEE Trans. Microw. Theory Techn.*, vol. 54, no. 3, pp. 1096–1106, Mar. 2006.

[21] A. Grebennikov, "Load Network Design Technique for Class F and Inverse Class F PAs", *High Frequency Electronics*, pp. 58-76, May 2011

[22] S. D. Kee, I. Aoki, A. Hajimiri, D. Rutledge, "The class-E/F family of ZVS switching amplifiers," *IEEE Transactions on Microwave Theory and Techniques,* vol. 51, no. 6, pp. 1677-1690, June 2003.

[23] R. A. Beltran, "Class-F and inverse class-F power amplifier loading networks design based upon transmission zeros," *IEEE MTT-S International Microwave Symposium (IMS)*, 2014, pp. 1-4, 1-6 June 2014.

[24] J. M. Rollett, "Stability and power–gain invariants of linear twoports," *Ins. Radio Engineers Trans, on Circuit Theory*, vol. 9, pp. 29–32, 1962.

[25] R. E. Collin, *Foundations for microwave engineering*, 2nd ed. John Wiley & Sons Inc., 2001.

[26] J. Guckenheimer, P. Holmes, *Nonlinear oscillations, dynamical systems and bifurcations of vector fields*, New York: Springer–Verlag, 1990.

[27] S. Mons, J.–C. Nallatamby, R. Queré, P. Savary, and J. Obregon, "A unified approach for the linear and nonlinear stability analysis of microwave circuits using commercially available tools," *IEEE Trans. Microw. Theory Techn.*, vol. 47, no. 12, pp. 2403–2409, Dec., 1999.

[28] A. Anakabe, J. M. Collantes, J. Portilla, et al. "Analysis and elimination of parametric oscillations in monolithic power amplifiers," *IEEE MTT–S Int. Microwave Symp*. Dig., Seattle, WA, Jun. 2002, pp. 2181–2184.

[29] W. Struble, A. Platzker, "A rigorous yet simple method for determining stability of linear N–port networks [and MMIC application]," *Gallium*

Arsenide Integrated Circuit (GaAs IC) Symposium Technical Digest, pp. 251–254, 1993.
[30] W. Struble, A. Platzker, "Rigorous determination of the stability of linear n–node circuits from network determinants and the appropriate role of the stability factor K of their reduced two–ports," *International Workshop on Integrated Nonlinear Microwave and Millimeterwave Circuits*, pp.93–107, 5–7 Oct., 1994.
[31] J. M. Paillot, J. C. Nallatamby, M. Hessane, R. Quéré, M. Prigent and J. Rousset, "A general program for steady state, stability, and FM noise analysis of microwave oscillators," *IEEE MTT-S Int. Microwave Symp.,* 1990, pp. 1287–1290.
[32] V. Rizzoli, F. Mastri and D. Masotti, "General noise analysis of nonlinear microwave circuits by the piecewise harmonic balance technique," *IEEE Trans. Microw. Theory Techn.*, vol. 42, pp. 807–819, May, 1994.
[33] L. Pantoli, A. Suárez, G. Leuzzi, F. Di Paolo, " Complete and systematic simulation tools for frequency divider design," *IEEE Trans. Microw. Theory Techn*., vol. 56, no. 11, pp. 2442–2452, Nov., 2008.
[34] D. Woods, "Reappraisal of the unconditional stability criteria for active 2-port networks in terms of S parameters," *Circuits and Systems, IEEE Transactions on* , vol.23, no. 2, pp. 73–81, Feb., 1976.
[35] R. W. Jackson, "Rollet proviso in the stability of linear microwave circuits – A tutorial." *IEEE Trans. on. Microwave Theory and Techniques*, vol. 54, no. 3, March. 2006, pp. 993-1000.
[36] J.F. Boehm and W.G. Albright, "Unconditional stability of a three-port network characterized with S–parameters," *IEEE Trans. Microw. Theory Techn.,* vol. 35, no. 6, pp. 582–586, Jun., 1987.
[37] E.L. Tan, "Simplified graphical analysis of linear three-port stability," *IEE Proc. Microw. Ant. and Propag*., vol. 152, no. 4, pp. 209–213, Aug., 2005.
[38] M. L. Edwards and J. H. Sinsky, "A new criterion for linear 2–port stability using geometrically derived parameters," *IEEE Trans. Microw. Theory Techn*., vol. 40, no. 12, pp. 2303–2311, Dec., 1992.
[39] J.M. Collantes, I. Lizarraga, A. Anakabe, J. Jugo. "Stability verification of microwave circuits through Floquet multiplier analysis," *2004 IEEE APCCAS*, Taiwan, 2004, pp. 997–1000.
[40] F. Bonani and M. Gilli, "Analysis of stability and bifurcations of limit cycles in Chua's circuit through the harmonic–balance approach," *IEEE Trans Circuits and Systems–I*, vol. 46, pp. 881–890, Aug., 1999.
[41] A. Suárez, *Analysis and design of autonomous microwave circuits*, IEEE–Wiley, Jan. 2009.
[42] F. Di Paolo, G. Leuzzi, "Bifurcation synthesis by means of Harmonic Balance and Conversion Matrix," *Proceedings of the European Gallium Arsenide Applications Symposium*, Munich, Oct., 2003, pp.521–524.

Almudena Suárez (M'96–SM'01–F'12) was born in Santander, Spain. She received the Electronic Physics and Ph.D. degrees from the University of Cantabria, Santander, Spain, in 1987 and 1992, respectively, and the Ph.D. degree in electronics from the University of Limoges, Limoges, France, in 1993.

She is currently a Full Professor with the Communications Engineering Department, University of Cantabria. She co-authored *Stability Analysis of Nonlinear Microwave Circuits* (Artech House, 2003) and authored *Analysis and Design of Autonomous Microwave Circuits* (IEEE-Wiley, 2009).

Prof. Suárez is a member of the Technical Committees of the IEEE Microwave Theory and Techniques Society (IEEE MTT-S) International Microwave Symposium (IMS) and the European Microwave Conference. She was an IEEE Distinguished Microwave Lecturer from 2006 to 2008. She is a member of the Board of Directors of the *European Microwave Association*. She is the Editor-in-Chief of the International Journal of Microwave and Wireless Technologies (Cambridge University Press). She was the co-chair of IEEE Topical Conference on RF Power Amplifiers (PAWR) in 2014 and 2015.

Franco Ramírez was born in Potosí, Bolivia. He obtained a degree in electronic systems engineering degree from the Military School of Engineering (EMI) in La Paz, Bolivia, in 2000 and the Ph.D. degree in communications engineering from the University of Cantabria, Santander, Spain in 2005. From 1999 to 2000 he worked for Ericsson de Bolivia Telecomunicaciones, where he was involved in several projects related with GSM and TDMA technologies. At present he is an Associate Professor at the Communications Engineering Department of the University of Cantabria. His research interests include phase noise, stability and the development of nonlinear techniques for the analysis and design of autonomous microwave circuits.

Sergio Sancho was born in Santurce, Spain, in 1973. In 1997 received the degree in Physics from Basque Country University. In 1998 he joined the Communications Engineering Department of the University of Cantabria, Spain, where he received the Ph.D. degree in Electronic Engineering in February 2002. At present, he works at the University of Cantabria, as an Associate Professor of its Communications Engineering Department. His research interests include the nonlinear analysis of microwave autonomous circuits and frequency synthesizers, including stochastic and phase–noise analysis.